Supplementary information on:

Temperature dependence of O solubility in liquid Na by atomistic simulations of Na(l)–Na_2O(s) interfaces using corrected machine-learning potential: A step towards simulating Na combustion

Chaeyeong Kim and Takuji Oda*

Department of Nuclear Engineering, Seoul National University, 1 Gwanak-ro, Gwanak-gu, Seoul 08826, South Korea

S1. Details of the atomic data used as the training set of the supervised learning

To prepare the training set of the supervised learning, density functional theory (DFT) calculations were done by using Vienna Ab initio Simulation Package (VASP)[1] on various systems that may appear in target molecular dynamics (MD) simulations. Table S1 shows detailed information on the systems included in the training set. The DFT calculation settings are given in the main text. Since our target systems are liquid Na, solid Na_2O and their interfaces, first-principles molecular dynamics (FPMD) simulations with *NVT* ensembles were performed on perfect solid Na_2O, solid Na_2O with vacancies, liquid pure Na and liquid Na with various O impurity concentrations. Additionally, liquid Na surfaces were included to prevent the formation of unrealistic clusters or voids in liquid Na and liquid Na_2O systems were included to avoid the melting of solid Na_2O at low temperature. FPMD simulations were also performed at interfaces between liquid Na and solid Na_2O crystal of (100), (110) or (111) orientation, and the data were included in the training set. Except for the interface and surface systems, four or five volumes were applied for each temperature in each system to increase the transferability of the ML potential. Additionally, for the same reason, simulations at very high temperature such as 2000 and 4000 K were included. In these high-temperature simulations, only one volume was applied for each case, since fair accuracy is sufficient for these conditions. Lastly, the data of static calculations of isolated Na and O atoms in a vacuum were added.

Table S1. Details of the data computed by the DFT calculation for the use in the supervised learning.

Reference Data			Number of configurations	
Solid	Perfect solid Na_2O	✓ Static calculation ✓ Strain was applied in xx and xy directions.	203	1443
		✓ *NVT*, FPMD ✓ 300 K, 1200 K	800	
	Solid Na_2O containing 3 vacancies ($2V_{Na}1V_O$)	✓ *NVT*, FPMD ✓ 300 K, 800 K, 1200 K	440	
Liquid	Liquid pure Na	✓ *NVT*, FPMD ✓ 600 K, 1000 K, 2000 K, 4000 K	1250	5600
	Liquid Na surface	✓ *NVT*, FPMD ✓ 600 K, 1000 K, 1500 K, 2000 K	1000	
	Liquid Na with O impurity	✓ *NVT*, FPMD ✓ O impurity concentrations: $Na_{101}O_1$, $Na_{100}O_2$, $Na_{98}O_4$, $Na_{96}O_6$, $Na_{94}O_8$, $Na_{92}O_{10}$ ✓ 600 K, 1000 K, 2000 K, 4000 K	2150	
	Liquid Na_2O	✓ *NVT*, FPMD ✓ 600 K, 1000 K, 2000 K, 4000 K	1200	
Interface	Interfaces between liquid Na and solid Na_2O	✓ *NVT*, FPMD ✓ 600 K, 1000 K, 1500 K, 2000 K ✓ Crystal orientation of Na_2O: (100), (110), (111)	1520	1520
Particles	Na/O atom	✓ Static calculation	2	2
Total			8565	8565

S2. Details of the numerical error correction applied to the DFT data

Since our target contains chemically and physically different systems, such as metals and insulators, system-specific settings were used in the DFT calculation with respect to the plane wave cutoff energy, reciprocal space sampling grid and smearing method, as mentioned in Section 2.1.2 of the main text. Thus, different magnitudes of numerical errors might appear, and the numerical errors cannot be completely cancelled out between the systems. Details of the settings are listed in Table S2. To minimise the numerical errors, we first checked numerical convergence with respect to the plane wave cutoff energy and the reciprocal space sampling grid in a liquid Na system with an O impurity and a perfect solid Na_2O system. The results are shown in Figure S1. The energy in the liquid Na system with an O impurity was not sufficiently converged with the 2×2×2 Monkhorst-Pack sampling gird,[2] and the energy in the perfect solid Na_2O system was not sufficiently converged with an energy cutoff of 400 eV. The differences between the results obtained by these settings used as our default settings and the converged results obtained by more accurate settings were greater than an energy root-mean-square error (RMSE) of our MTP, 2.0 meV/atom. According to Figure S1, at least the $5 \times 5 \times 5$ Monkhorst-Pack sampling gird[2] should be used for the liquid system, and an energy cutoff of 700 eV should be adopted for the solid system to suppress the residual numerical error below the MTP fitting error.

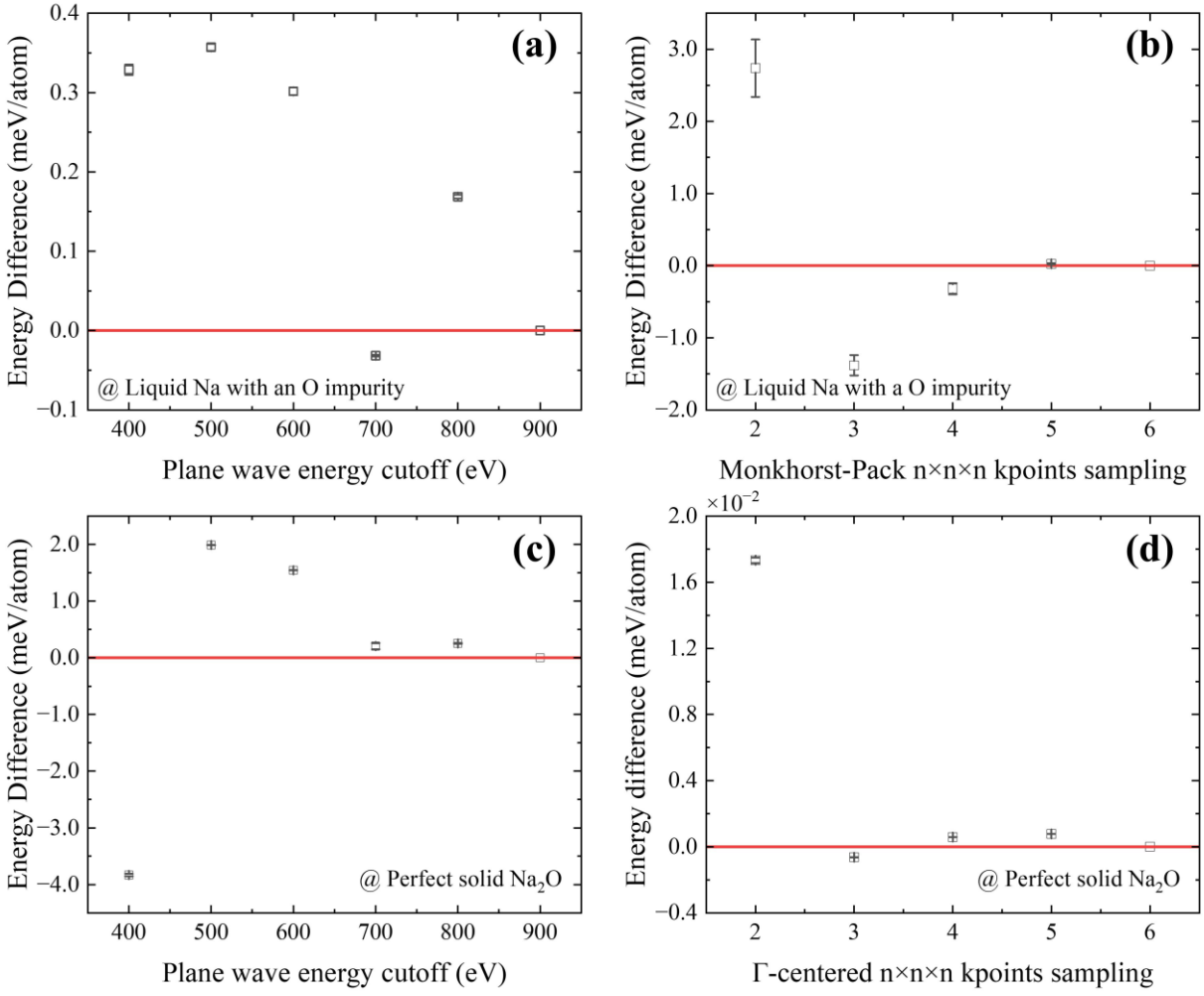

Figure S1. Energy convergence of DFT calculation in the system of liquid Na containing an O impurity for (a) the plane-wave energy cutoff and (b) the Monkhorst-Pack reciprocal space sampling grid. (c) and (d) show the energy convergence in the solid Na_2O system for the plane-wave energy cutoff and the Γ-centered reciprocal space sampling grid, respectively. The energy difference was calculated by referring to the energy calculated with an energy cutoff of 900 eV and a sampling grid of 6×6×6. The red line indicates no difference from the reference, and the error bar denotes standard deviations determined from three different configurations for each case.

To remove the numerical errors efficiently, the raw DFT calculation results were empirically corrected by subtracting quantified numerical errors from the energy and the diagonal elements of the stress tensor calculated by the default settings. The energy/stress numerical errors were quantified from the differences between the default and correction settings, and five configurations were used in each system to average the differences and estimate their standard deviations. For the correction settings, more accurate Fast Fourier Transform (FFT) settings including denser FFT meshes (PREC=Accurate) and energy cutoff of 800 eV were adopted for all systems. As for the reciprocal space sampling grid, 5×5×5 Monkhorst-Pack grids[2] were used for cubic liquid systems, and 5×5×1 grids were used for liquid Na surface and interface systems, which had a long shape in the z-direction. As errors could depend on the volume, temperature, phase and O concentration, a total of 132 different systems were evaluated. Figure S2 shows their averages and standard deviations. The range of standard deviation is acceptable to correct the errors with this empirical method since the magnitudes are much less than RMSEs of MTP, which were 2.0 meV/atom for energy and 1.8 kbar for stress. Note that the numerical force error was not corrected, since its size is usually small because the force is calculated as a derivative of energy, by which the numerical error in the energy can be largely cancelled out. Off-diagonal elements of stress tensors were also not corrected, because Pulay stress, which is the stress error due to a small energy cutoff, is usually small for off-diagonal elements. All static calculations were performed with accurate settings that were used to calculate the reference energy/stress in the numerical error correction. Thus, the numerical corrections were not applied to static calculation data.

Table S2. Default settings used in FPMD calculations and correction settings used to calculate the reference energy/stress in the numerical error correction.

Reference Data		Default setting			Correction setting		
		PREC	**ENCUT**	**KPOINTS**	**PREC**	**ENCUT**	**KPOINTS**
Solid	Perfect solid Na_2O	Normal	400 eV	Γ-centered 3×3×3	Accurate	800 eV	Γ-centered 3×3×3
	Solid Na_2O containing 3 vacancies ($2V_{Na}1V_O$)	Normal	400 eV	Γ-centered 3×3×3	Accurate	800 eV	Γ-centered 3×3×3
Liquid	Liquid pure Na	Normal	400 eV	Monkhorst-Pack 2×2×2	Accurate	800 eV	Monkhorst-Pack 6×6×6
	Liquid Na surface	Normal	400 eV	Monkhorst-Pack 2×2×1	Accurate	800 eV	Monkhorst-Pack 5×5×1
	Liquid Na with O impurity	Normal	400 eV	Monkhorst-Pack 2×2×2	Accurate	800 eV	Monkhorst-Pack 6×6×6
	Liquid Na_2O	Normal	400 eV	Γ-centered 3×3×3	Accurate	800 eV	Γ-centered 5×5×5
Interface	Interfaces between liquid Na and solid Na_2O	Normal	400 eV	Γ-centered 3×3×1	Accurate	800 eV	Γ-centered 5×5×1

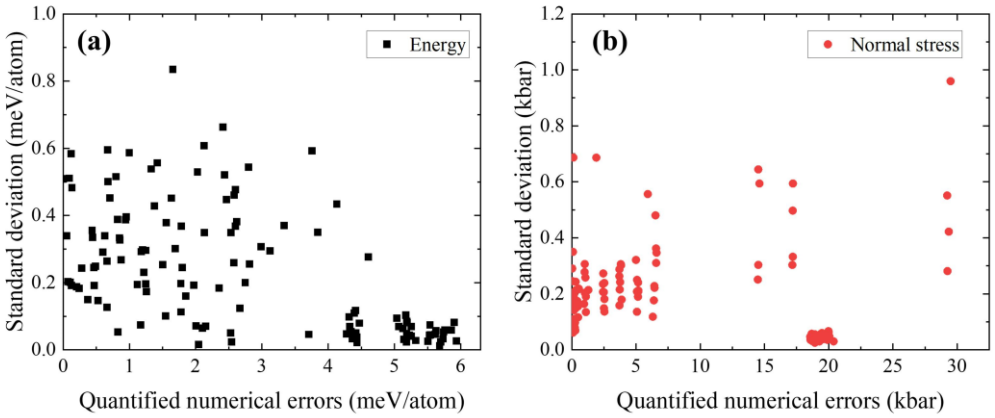

Figure S2. Numerical errors and their standard deviations in (a) the energy and (b) the diagonal elements of the stress tensor. All standard deviations are less than the RMSEs of the present MTP, which were 2.0 meV/atom for energy and 1.8 kbar for stress.

S3. Moment Tensor Potential (MTP) and hyperparameter optimisation

In this study, MTP was constructed using the MLIP package.[3] In MTP[4], the energy contribution of a local environment of each atom, $\mathrm{V}(n_i)$, is expressed by a linear combination of basis functions as follows:

$$\mathrm{V}(n_i) = \sum_\alpha \xi_\alpha \mathrm{B}_\alpha(n_i), \tag{S1}$$

where n_i is the local atomic environment of i^{th} atom, $\{\xi_\alpha\}$ is a parameter set, optimised by training through the reference database (training set) and $\{\mathrm{B}_\alpha\}$ is a set of basis functions. The basis functions are formed as contractions of one or more moment tensor descriptors $M_{\mu,\nu}$, named *moments*, which are consisted of radial and angular parts as

$$M_{\mu,\nu}(n_i) = \sum_j f_\mu\left(|r_{ij}|, z_i, z_j\right) f_\nu(\boldsymbol{r}_{ij}), \tag{S2}$$

where $f_\mu\left(|r_{ij}|, z_i, z_j\right)$ is the radial part, $f_\nu(\boldsymbol{r}_{ij})$ is the angular part, μ and ν are the indices of the radial and angular parts, respectively, $\boldsymbol{r}_{ij}$ is the position of the j^{th} atom relative to the i^{th} atom and z_i and z_j are the atomic types of the i^{th} and j^{th} atoms, respectively. All contractions of one or more *moments* $M_{\mu,\nu}$ whose levels are less than a hyperparameter $lev_{\max}$, called *maximum level* or *level of MTP*, are included as the basis functions, $\{\mathrm{B}_\alpha\}$. The level of $M_{\mu,\nu}$ is defined as

$$lev\, M_{\mu,\nu} = 2 + 4\mu + \nu. \tag{S3}$$

The radial part of $M_{\mu,\nu}$ has the form of a linear combination of radial basis functions, $Q^{(\beta)}$, as

$$f_\mu\left(|r_{ij}|, z_i, z_j\right) = \sum_\beta^{N_Q} c^{(\beta)}_{\mu,z_i,z_j}\, Q^{(\beta)}\left(|r_{ij}|\right), \tag{S4}$$

where $c^{(\beta)}_{\mu,z_i,z_j}$ is a set of radial parameters, β is the index of the radial basis function, and N_Q is the number of the radial basis functions. As the radial basis functions, Chebyshev polynomials multiplied by a damping function in the spatial range from the minimal cutoff ($R_{\min}$) to the maximal cutoff ($R_{\max}$) were used.

The angular part is a tensor using outer products of $\boldsymbol{r}_{ij}$ as

$$f_\nu(\boldsymbol{r}_{ij}) = \boldsymbol{r}_{ij} \underbrace{\otimes \ldots \otimes}_{\nu\ times} \boldsymbol{r}_{ij} \tag{S5}$$

where $\otimes$ denotes the outer product and ν is the number of outer products.

The three hyperparameters, lev_{max}, R_{max} and N_Q, are highly related to the accuracy and computational speed of an MTP. The larger hyperparameters could decrease training errors while slowing down MD simulations. Therefore, the hyperparameters need to be determined considering a balance between calculation accuracy and speed. The accuracy is about the reproductivity of the DFT calculations, not the reproductivity of experimental data and was defined as the energy root-mean-square error (RMSE) of the MTP for the training database. The speed was quantified by the MD computational speed of MTP for LAMMPS[5] calculations. Since an MTP is trained by non-linear iterative optimisation in the MLIP package, the performance is also affected by initial model coefficients, which are randomly generated. To account for this effect, the training error with each hyperparameter set was determined with five MTPs of different initialization of model coefficients. The computational speed was measured by performing MD simulations on the interfacial system containing 189 atoms between liquid Na and solid Na_2O of (100) orientation using a calculational server of two Intel® Xeon® Gold 6130 CPUs (32 cores in total). For each hyperparameter set, the computational speed was determined by averaging the results of five MD simulations with different initial velocities. As shown in Figure S3, increasing the hyperparameters improves accuracy while slowing down MD simulations. Consequently, we selected lev_{max} = 16, R_{max} = 6 Å and N_Q = 8, which can achieve a training error of 2 meV/atom at an affordable computational cost.

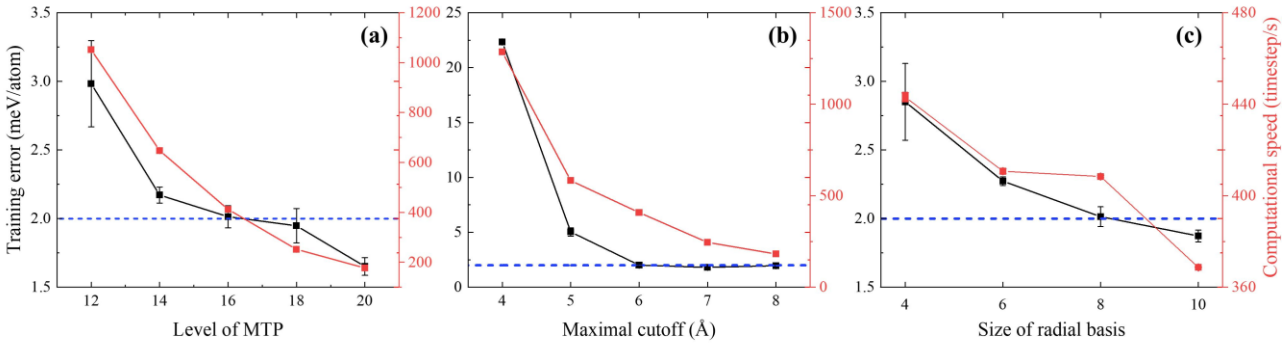

Figure S3. Training error and computational speed of the MTPs as a function of (a) level of MTP (lev_{max}), (b) maximal cutoff (R_{max}) and (c) the number of radial basis (N_Q). The default values were set to lev_{max} = 16, R_{max} = 6 Å and N_Q = 8 in these tests, and only one parameter was changed in each test. The blue dashed lines indicate 2 meV/atom in the training error.

S4. Definition of extrapolation grade

This section describes the concept and definition of extrapolation grade with reference to what is reported in Ref. [3]. The extrapolation grade is a measure of how much a given configuration is extrapolated. In the MLIP package,[3] the extrapolation grade is calculated based on the D-optimality criterion. The criterion assumes that the submatrix with the greatest determinant contains the most extreme and diverse information out of all possible submatrices that can be created from the training set. The energy of a system in MTP $\mathrm{E}^{\mathrm{mtp}}$ is determined as expressed in the equation below,

$$\mathrm{E}^{\mathrm{mtp}}(cfg;\xi) = \sum_{i=1}^{n} \mathrm{V}(n_i) = \sum_{i=1}^{n}\sum_{\alpha=1}^{m} \xi_\alpha \mathrm{B}_\alpha(n_i) = \sum_{\alpha=1}^{m} \xi_\alpha \sum_{i=1}^{n} \mathrm{B}_\alpha(n_i) = \sum_{\alpha=1}^{m} \xi_\alpha b_\alpha(cfg), \tag{S6}$$

where $\{b_\alpha(cfg)\}$ is a set of basis function of a system, n is the number of atoms in a system and m is the number of MTP parameters.

Since the number of configurations included in the training set (represented by k) is generally much greater than the number of MTP parameters (represented by m), the system of equations is overdetermined as follows:

$$\begin{pmatrix} E^{mtp}(cfg_1) & \dots & E^{mtp}(cfg_k) \end{pmatrix} = \begin{pmatrix} \xi_1 & \dots & \xi_m \end{pmatrix} \begin{pmatrix} b_1(cfg_1) & \cdots & b_1(cfg_k) \\ \vdots & \ddots & \vdots \\ b_m(cfg_1) & \cdots & b_m(cfg_k) \end{pmatrix}. \tag{S7}$$

The method of determining the extrapolation grade involves selecting a set of m representative configurations from the training set, called the active set. The active set, which is based on D-optimality, contains configurations with the largest determinant and is considered to be the most informative submatrix among all submatrices that can be constructed from the training set.

When a new configuration is generated by classical molecular dynamics, the extrapolation can be judged by whether the determinant increases as the configuration replaces a row in the active set. The extrapolation grade, denoted by γ(cfg), is defined as

$$\gamma(\mathrm{cfg}) = \max_{1\le j\le m}|c_j|, \qquad where\ (c_1 \quad \cdots \quad c_m) = (b_1 \quad \cdots \quad b_m)\mathbf{A}^{-1}, \tag{S8}$$

where $(b_1 \quad \cdots \quad b_m)$ is a set of basis functions of the new configuration and $\mathbf{A}^{-1}$ is the inverse matrix of active set. Thus, γ(cfg) greater than 1.0 indicates the active set can be extended by replacing the row of index $j_{\max}$ with the row of the newly generated configuration. The $j_{\max}$ can be determined as

$$\mathrm{j_{max}} = \mathrm{argmax}_{1\le \mathrm{j}\le \mathrm{m}}|c_j|. \tag{S9}$$

If the number of configurations in the active set is equal to that of the training set, MTP parameters can be obtained by solving the determined system and as

$$\boldsymbol{\xi} = (E^{qm}(cfg_1) \quad \ldots \quad E^{qm}(cfg_m))\mathbf{A}^{-1}, \tag{S10}$$

where $E^{qm}(cfg_i)$ is energy calculated by quantum mechanical simulation on the i^{th} configuration.

The MTP energy of any configuration can be expressed as a linear combination between a parameter set $\{c\}$ and a set of quantum computational energy contained in the training set $\{E^{qm}\}$ as

$$\mathrm{E^{mtp}}(cfg;\xi) = \sum_{i=1}^{n}\sum_{\alpha=1}^{m}\xi_\alpha \mathrm{B}_\alpha(n_i) = \sum_{j=1}^{m} c_j E^{qm}(cfg_j). \tag{S11}$$

From the above equation, if any *c* parameter of a new configuration is larger than 1.0, the configuration is considered an extrapolation from quantum mechanical calculations. Otherwise, it is considered interpolated. Therefore, in the MLIP package, they interpreted γ(cfg) as the extrapolation grade.

S5. Effects of active learning on MTP performance in this study

We obtained 16 configurations through active learning and then used them to retrain the MTP. Although this number is small compared to the size of the initial training set (8565 configurations), the extrapolation grade of the interface systems was significantly reduced. As explained in section S4, the grade is determined by referring only to the active set, which consists of a subset of the training set with the number of configurations equal to the number of MTP parameters. In this study, the MTP had 211 parameters with lev_{max} = 16 and N_Q = 8, so 211 configurations were chosen for the active set. Table S3 shows the number and percentage of $Na_{(l)}$–$Na_2O_{(s)}$ interface systems selected as components of the active set before and after active learning. The addition of the 16 configurations increased the proportion of the interface systems in the active set by about 3 %, decreasing the extrapolation grades of the interface systems. In the 2nd iteration of active learning, all configurations held extrapolation grades less than 2.1, so we stopped active learning.

Table S3. The number and proportion of configurations of $Na_{(l)}$–$Na_2O_{(s)}$ interfaces in the active set before and after active learning. The percentage in parentheses represents the proportion of the selected interface configurations in the active set relative to the total of 211 configurations.

Orientation of $Na_2O_{(s)}$ at $Na_{(l)}$–$Na_2O_{(s)}$ interfaces	MTP before active learning	MTP after active learning
(100)	7 (3.3%)	10 (4.7%)
(110)	7 (3.3%)	6 (2.8%)
(111)	2 (0.9%)	7 (3.3%)
Total	16 (7.6%)	26 (10.9%)

Table S4 shows the extrapolation grades of the 16 selected configurations and the energy error of MTP before and after active learning compared to the DFT calculations. The selected configurations had extrapolation grades of 2.1 or higher as designed, with a maximum and average value of 2.42 and 2.18, respectively. The energy errors of MTP for the selected configurations were comparable to the maximal energy training error of the initial MTP obtained by the supervised learning, 2.19 eV/system (or 21.45 meV/atom). This indicates that active learning successfully identified the atomic

environments that were not included in the initial MTP training set. In fact, by adding these selected configurations to the training set and rebuilding the MTP, the energy errors of the selected configurations were reduced.

Strictly speaking, even after active learning, we cannot conclusively judge whether all relevant atomic environments were thoroughly included in the training set. Nevertheless, as confirmed in this section, active learning successfully worked as designed, and no additional configurations were selected in the 2nd cycle of active learning, as mentioned in the main text. In addition, the MTP trained with supervised and active learning achieved good reproductivity of DFT calculations, as presented in the main text. Therefore, we concluded that no additional active learning with a stricter criterion, such as 1.5 as the threshold for new configurations selection, would not be needed for the purpose of the present study.

Table S4. Extrapolation grades of the configurations selected through active learning and the energy errors of MTP before and after active learning by reference to the DFT calculations

The ID of selected configurations	γ(cfg)	MTP before active learning		MTP after active learning	
		Absolute per-system energy error (eV/system)	Absolute per-atom energy error (meV/atom)	Absolute per-system energy error (eV/system)	Absolute per-atom energy error (meV/atom)
1	2.10	3.47	18.38	2.18	11.54
2	2.10	3.41	18.06	2.20	11.63
3	2.42	3.22	17.03	2.02	10.70
4	2.14	3.02	15.99	2.04	10.77
5	2.15	2.80	14.84	1.59	8.43
6	2.12	3.29	17.39	2.24	11.85
7	2.10	3.10	16.38	1.68	8.88
8	2.12	2.59	13.68	1.70	8.97
9	2.32	1.99	17.49	1.40	12.25
10	2.22	1.58	13.82	0.99	8.66
11	2.11	1.94	17.03	1.33	11.69
12	2.11	1.44	12.66	0.75	6.60
13	2.17	1.70	14.91	1.04	9.14
14	2.13	1.18	10.33	0.83	7.26
15	2.33	1.40	12.31	0.79	6.93
16	2.19	1.66	14.56	1.10	9.62
Mean	**2.18**	**2.36**	**15.30**	**1.49**	**9.68**

S6. MD simulation details

In this study, fundamental material properties of liquid Na and solid Na_2O as well as the diffusion coefficients of Na and O and Na_2O solution enthalpy in liquid Na were calculated by using the constructed MTPs. Detailed calculation settings are provided below.

Density, isothermal compressibility and radial distribution function (RDF) of liquid pure Na were calculated with cubic simulation cells composed of 816 Na atoms. All quantities were determined after reaching the equilibrium. The average density and its standard error of the mean (SEM) were determined from 20 NPT simulations of different initial velocities for each temperature. The isothermal compressibilities were calculated from a second-order polynomial fit to pressure–volume relation. To derive the relation at each temperature, for five different volumes, the average pressure at each volume was determined from 10 *NVT* simulations of different initial velocities. The RDF was determined by averaging RDF profiles for 10 ps.

Bulk Na_2O properties at room temperature, such as bulk modulus and lattice constant, were determined by fitting the pressure–volume relation to the third-order Birch–Murnaghan (BM) equation of state (EOS). To obtain the pressure–volume relation, *NVT* simulations were performed with 3×3×3 supercells ($Na_{216}O_{108}$). For direct comparison with experimental data, volumes consistent with that of experimentally reported pressure–volume relation were applied. For each volume, five samples were prepared with different initial velocities, and then the average pressure was determined. The properties of solid Na_2O at 0 K were obtained by geometry optimization calculations and static calculations.

Self-diffusion coefficient of Na and diffusion coefficient of O in liquid Na were calculated at 500, 600 and 1000 K. As mentioned in Section 2.2.3 of the main text, various system sizes were used. To obtain the three-dimensional coefficients using the Einstein relation from mean square displacement (MSD), 100 *NPT* simulations starting with different initial atomic

velocities were performed. In each *NPT* simulation, MSD was calculated every 1 ps for 20 ps after reaching the equilibrium. From these 100 data, the average value and its SEM of diffusion coefficient were calculated at each temperature.

Solution enthalpy was calculated by Eq. (8) of the main text using enthalpies of liquid pure Na system, liquid Na containing O impurities system and perfect solid Na_2O system. The enthalpy for each system was averaged for dozens of independent samples before calculating the solution enthalpy. The number of samples for each temperature was determined so that comparable SEMs can be achieved for all conditions. To be specific, 20, 40, 60 and 80 samples were employed at 400–500 K, 600–700 K, 800–900 K and 1000 K, respectively. Similarly, the enthalpies of perfect solid Na_2O were averaged over 5, 10, 15 and 20 samples, respectively.

S7. Equilibrium simulation for solubility calculation using the direct coexisting method (DCM)

Since kinetics becomes faster at higher temperatures, different equilibrium times were applied depending on the temperature to efficiently calculate the solubility by DCM. Specifically, equilibrium simulations were performed for 15, 11 and 7 ns at 800, 900 and 1000 K, respectively, and the solubility was estimated for 1 ns after reaching the equilibrium at each temperature. As mentioned in Section 2.2.4 of the main text, the solubility was determined based on the averaged Na and O densities over the z coordinate [75 Å, 175 Å], where Na atoms were liquid and O atoms were solutes. Figure S4 shows the number of O atoms in this region as a function of simulation time for three samples during equilibrium simulations at each temperature. The green curve indicates the averaged values over the three samples. It is confirmed that the number of solute O atoms reasonably converged within 15, 11 and 7 ns at 800, 900 and 1000 K, respectively.

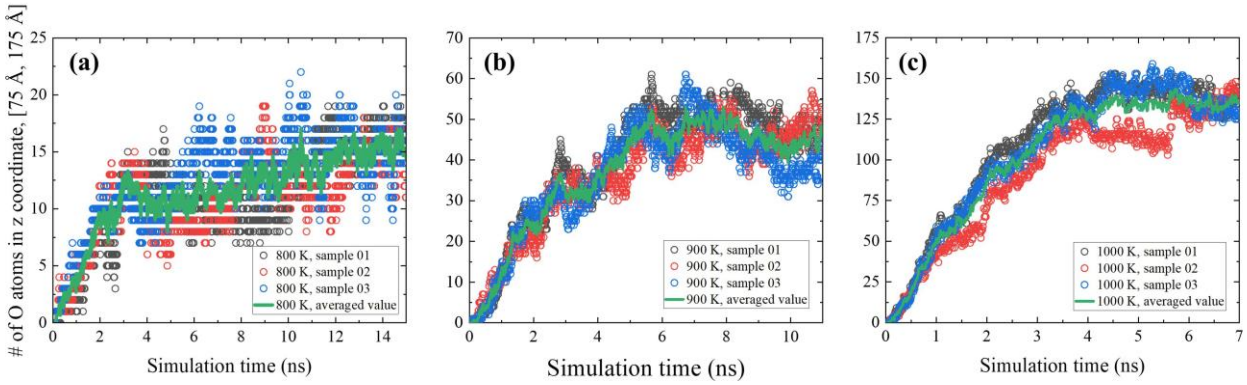

Figure S4. The number of dissolved O atoms in liquid Na region where the z coordinate is [75 Å,175 Å] as a function of simulation time at (a) 800 K, (b) 900 K and (c) 1000 K in the DCM calculations using C_{0035}.

S8. Derivation of the thermodynamic model of dilute solution

To derive Eqs. (11)–(13) used in Section 2.2.5 of the main text, we consider two systems in which liquid Na is in contact with solid Na_2O as shown in Figure S5. One is a liquid Na system with O dissolved to the solubility limit, and the other is a system with one additional O atom (or, more precisely, one additional unit of Na_2O) dissolved. Both systems contain the same number of Na and O atoms. The former and the later systems are referred to as system-1 and system-2 in the following.

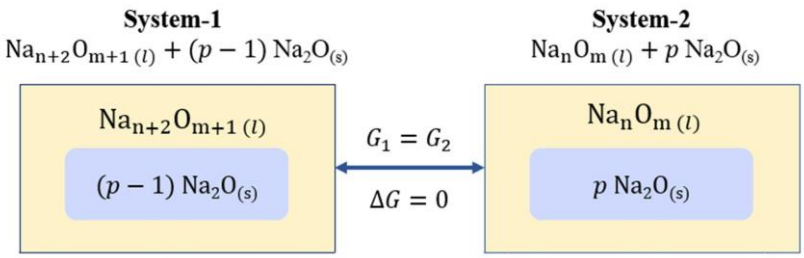

Figure S5. Equilibrium condition for a solution where O solubility limit is reached. G_1 and G_2 denote the Gibbs free energies of system-1 and system-2, respectively.

The Gibbs free energy difference between system-1 and system-2 should be zero at equilibrium where the O concentration reaches the solubility limit. Here, the Gibbs energy difference can be written down by the enthalpy difference and entropy difference as follows:

$$\Delta G_{sol}(T) = G_2(T) - G_1(T) = \Delta H_{sol}(T) - T\left(\Delta S_{sol}^{conf.}(T) + \Delta S_{sol}^{w/o\ conf.}(T)\right) = 0, \quad \text{(S12)}$$

where $G_1(T)$ is the Gibbs free energy of system-1 and $G_2(T)$ is the Gibbs free energy of system-2. $\Delta H_{sol}(T)$ is the enthalpy difference, $\Delta S_{sol}^{conf.}(T)$ is the configurational entropy difference and $\Delta S_{sol}^{w/o\ conf.}$ is the entropy difference, excluding the configurational entropy term, between system-1 and system-2.

In a thermodynamic model, interface effects are usually ignored assuming that both liquid Na and solid Na_2O are infinitely large. Accordingly, the Gibbs free energies of system-1 and system-2 can be described as

$$G_1 = G_{Na_nO_m(l)} + pG_{Na_2O(s)}, \quad \text{(S13)}$$

$$\mathrm{G}_2 = G_{Na_{n+2}O_{m+1}(l)} + (p-1)G_{Na_2O(s)}, \quad \text{(S14)}$$

where $G_{Na_nO_m(l)}$ is the Gibbs free energy of a solution containing n Na and m O atoms, $G_{Na_{n+2}O_{m+1}(l)}$ is the Gibbs free energy of a solution containing $n+2$ Na and $m+1$ O atoms, and $G_{Na_2O(s)}$ is the Gibbs free energy of a unit of solid Na_2O.

Substituting Eqs. (S13) and **(**S14) to Eq. (S12), the differences in the Gibbs free energy, enthalpy and entropies can be represented as follows:

$$\Delta G_{sol} = G_{Na_{n+2}O_{m+1}(l)} - G_{Na_nO_m(l)} - G_{Na_2O(s)}, \quad \text{(S15)}$$

$$\Delta H_{sol} = H_{Na_{n+2}O_{m+1}(l)} - H_{Na_nO_m(l)} - H_{Na_2O(s)}, \quad \text{(S16)}$$

$$\Delta S_{sol}^{w/o\ conf.} = S_{Na_{n+2}O_{m+1}(l)}^{w/o\ conf.} - S_{Na_nO_m(l)}^{w/o\ conf.} - S_{Na_2O(s)}^{w/o\ conf.}, \quad \text{(S17)}$$

$$\Delta S_{sol}^{conf.} = S_{Na_{n+2}O_{m+1}(l)}^{conf.} - S_{Na_nO_m(l)}^{conf.} - S_{Na_2O(s)}^{conf.}, \quad \text{(S18)}$$

where $H_{Na_{n+2}O_{m+1}(l)}$, $S_{Na_{n+2}O_{m+1}(l)}^{w/o\ conf.}$ and $S_{Na_{n+2}O_{m+1}(l)}^{conf.}$ are respectively the enthalpy, entropy excluding configurational entropy, and configurational entropy of the solution containing $n+2$ Na and $m+1$ O atoms, $H_{Na_nO_m(l)}$, $S_{Na_nO_m(l)}^{w/o\ conf.}$, and $S_{Na_nO_m(l)}^{conf.}$ are those of the solution containing n Na and m O atoms, and $H_{Na_2O(s)}$, $S_{Na_2O(s)}^{w/o\ conf.}$ and $S_{Na_2O(s)}^{conf.}$ are those of a unit of solid Na_2O.

To describe $\Delta S_{sol}^{conf.}$ based on Boltzmann's entropy formula, the following assumptions were applied.

1. The interaction between O solutes is negligible. This assumption is reasonable since the O solubility limit in liquid Na is low ($\chi_O \leq 0.03$ at 1000 K, based on the thermodynamic model with the optimal correction value, C_{003}) so it can be considered a dilute solution, approximately. In addition, the segregation of solute O atoms was rarely observed in the MD simulations performed in this study.

2. The configurational entropy of $Na_2O_{(s)}$ is negligible compared to those of the solutions. Since the target temperatures are sufficiently lower than the melting point of $Na_2O_{(s)}$ ($T_m = 1405$ K), defect concentration is expected to be kept low.
3. O solute atoms were treated in equivalent with Na atoms in a liquid state when calculating the configurational entropy.

Under these assumptions, $\Delta S_{sol}^{conf.}$ can be expressed as

$$\Delta S_{sol}^{conf.} = S_{Na_{n+2}O_{m+1}(l)}^{conf.} - S_{Na_nO_m(l)}^{conf.} = k_B\, ln\, {}_{n+m+3}\mathrm{C}_{m+1} - k_B\, ln\, {}_{n+m}\mathrm{C}_m. \tag{S19}$$

Since our solutions are dilute solutions ($n \gg m$ and $n \gg 1$), $\Delta S_{sol}^{conf.}$ can be further developed using Starling's approximation and finally expressed as a function of the mole fraction of O, $\chi_O(T)$, as

$$\Delta S_{sol}^{conf.}(T) \sim k_B\, ln\, \frac{n+m}{m} = k_B\, ln\, \frac{1}{\chi_O(T)}. \tag{S20}$$

Subsequently, we can relate $\chi_O(T)$ with $\Delta H_{sol}(T)$ and $\Delta S_{sol}^{w/o\ conf.}(T)$ by combining Eqs. (S12) and (S20):

$$ln\ \chi_O(T) = -\frac{\Delta H_{sol}(T) - T\Delta S_{sol}^{w/o\ conf.}(T)}{k_B T}. \tag{S21}$$

In the present study, MD simulations were performed in the solutions of 812 Na atoms and 4 O atoms to approximately obtain Na_2O solution enthalpy, ΔH_{sol}:

$$\begin{aligned} \Delta H_{sol} &= H_{Na_{n+2}O_{m+1}(l)} - H_{Na_nO_m(l)} - H_{Na_2O(s)} \\ &\approx \left(H_{Na_{812}O_4(l)} - H_{Na_{816}(l)} - 4H_{Na_2O(s)}\right)/4. \end{aligned} \tag{S22}$$

Although ΔH_{sol} obtained by Eq. (S22) is of the specific case (812 Na and 4 O), this ΔH_{sol} can be applied to Eq. (S21), approximately. This approximation is accurate if the O concentration is dilute enough to ignore interactions between solute O atoms. In such conditions, ΔH_{sol} is expected to be hardly dependent on m if n is reasonably large and the O concentration is sufficiently small (~0.005 in the atomic fraction in our calculation). Figure S6 shows ΔH_{sol} calculated as a function of the number of O atoms (m) in the solution used in MD simulations, keeping the total number of atoms in the solution to be 816, as $n + m =$ 816 where n is the number of Na atoms. ΔH_{sol} of all conditions show nearly the same value within the statistical precision. This confirms that ΔH_{sol} obtained by Eq. (S22) can be applied to Eqs. (S16) and (S21) without considering the dependence on n and m.

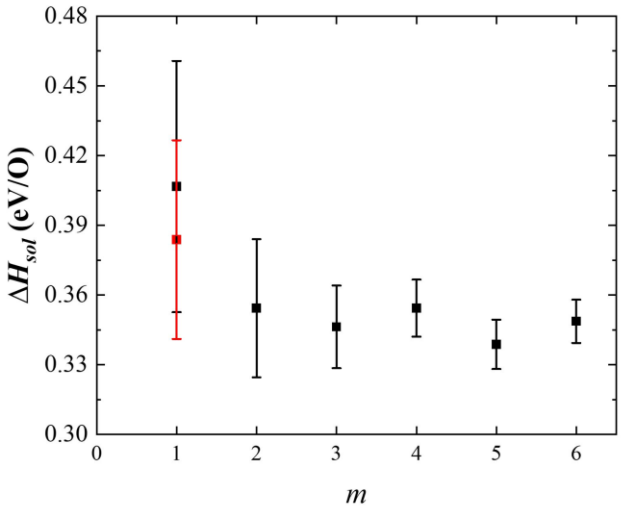

Figure S6. Calculated ΔH_{sol} as a function of the number of O atoms (m) in the solution used in MD simulations. All solutions were composed of n Na and m O atoms with the total number of atoms to be 816 as $n + m = 816$. The data point and error bar at each m are the average value of ΔH_{sol} and its SEM. The red-colored data and its SEM were obtained from 40 samples in the solution and 10 samples in solid Na_2O ($m = 1$) and the others were obtained from 20 samples in the solution and 5 samples in solid Na_2O.

The O solubility limit at a reference temperature T_0, $x_O(T_0)$, was calculated by the DCM as described in the main text. Subsequently, with $\Delta H_{sol}(T_0)$ obtained by Eq. (S22), we can determine $\Delta S_{sol}^{w/o\ conf.}$ at T_0 as

$$\Delta S_{sol}^{w/o\ conf.}(T_0) = k_B\, ln\ x_O(T_0) + \frac{\Delta H_{sol}(T_0)}{T_0}. \tag{S23}$$

To determine the O solubility limit at an arbitrary temperature T_1, $x_O(T_1)$, using Eq. (S21), we need to obtain $\Delta H_{sol}(T_1)$ and $\Delta S_{sol}^{w/o\ conf.}(T_1)$. $\Delta H_{sol}(T_1)$ can be calculated by Eq. (S22) based on MD simulation results. To obtain the entropy term, we first obtain the heat capacity of the solution of solid Na_2O in liquid Na, $\Delta C_p^{sol}(T)$, by partial derivative of the solution enthalpy as

$$\Delta C_p^{sol} = \frac{\partial \Delta H_{sol}(T)}{\partial T}. \tag{S24}$$

Here, $\Delta H_{sol}(T)$ obtained from 400 K to 1000 K with 100 K interval in MD simulations was first fitted to a linear function and its partial derivative for temperature was analytically evaluated.

Using thermodynamic relation, the total solution entropy at T_1, which is the summation of the non-configurational term and configurational term, is expressed as

$$\left\{\Delta S_{sol}^{w/o\ conf.}(T_1) + \Delta S_{sol}^{conf.}(T_1)\right\} = \left\{\Delta S_{sol}^{w/o\ conf.}(T_0) + \Delta S_{sol}^{conf.}(T_0)\right\} + \int_{T_0}^{T_1} \frac{\Delta C_p^{sol}(T)}{T} dT. \tag{S25}$$

Here, it is reasonable to assume that non-configurational entropy and solution enthalpy are independent of the O concentration, approximately, if the solution is dilute, as we confirmed above that ΔH_{sol} is hardly dependent on the composition. Thus, in Eq. (S25), if $\Delta C_p^{sol}(T)$ is derived from $\Delta H_{sol}(T)$ obtained with a fixed composition, the configurational entropy terms will disappear because the configurational entropy is dependent only on the composition, not on the temperature, i.e., $\Delta S_{sol}^{conf.}(T_1) = \Delta S_{sol}^{conf.}(T_0)$. In the present study, $\Delta H_{sol}(T)$ was obtained by Eq. (S16) with fixing the composition.

Consequently, with predetermined $\Delta S_{sol}^{w/o\ conf.}(T_0)$ and $\Delta C_p^{sol}(T)$, we can obtain $\Delta S_{sol}^{w/o\ conf.}(T_1)$ in dilute solution as follows:

$$\Delta S_{sol}^{w/o\ conf.}(T_1) = \Delta S_{sol}^{w/o\ conf.}(T_0) + \int_{T_0}^{T_1} \frac{\Delta C_p^{sol}(T)}{T} dT. \quad \text{(S26)}$$

Eqs. (S21), (S24) and (S26) are the same with Eqs. (11)–(13) of the main text.

S9. Optimisation of function form to fit solution enthalpy

In this work, we estimated the temperature dependence of O solubility from temperature-dependent solution enthalpy calculated by MD. The solution enthalpy was calculated from 400 to 1000 K with 100 K intervals and fitted to a linear equation. Since the heat capacity of the solution was determined by Eq. (12) in the main text and the solution entropy was calculated by Eq. (13) in the main text, these quantities as well as the temperature dependence of O solubility can be affected by the form of the fitting equation used to describe the temperature dependence of solution enthalpy. Therefore, we tested three fitting equations, namely, linear, third-order polynomial and logistic functions. In Figure S7, solution enthalpy (ΔH_{sol}), heat capacity of solution (ΔC_p^{sol}), solution entropy excluding configurational entropy ($\Delta S_{sol}^{w/o\ conf.}$) and Gibbs free energy of solution excluding configurational entropy ($\Delta G_{sol}^{w/o\ conf.}$), are shown as functions of temperature. The choice of the fitting equation significantly affected the temperature dependence of ΔC_p^{sol}. However, the effect was greatly reduced on the $\Delta S_{sol}^{w/o\ conf.}$ and $\Delta G_{sol}^{w/o\ conf.}$. Consequently, we confirmed that the effect of fitting equations on the O solubility calculation was negligible in a temperature range from 400 to 1000 K as shown in Figure S7(d). Since our target is mainly the O solubility and partly the enthalpy and entropy of the solution, not the ΔC_p^{sol}, the choice of the fitting equation is not very important. Thus, for simplicity, the linear equation was applied to fit the solution enthalpy in this study.

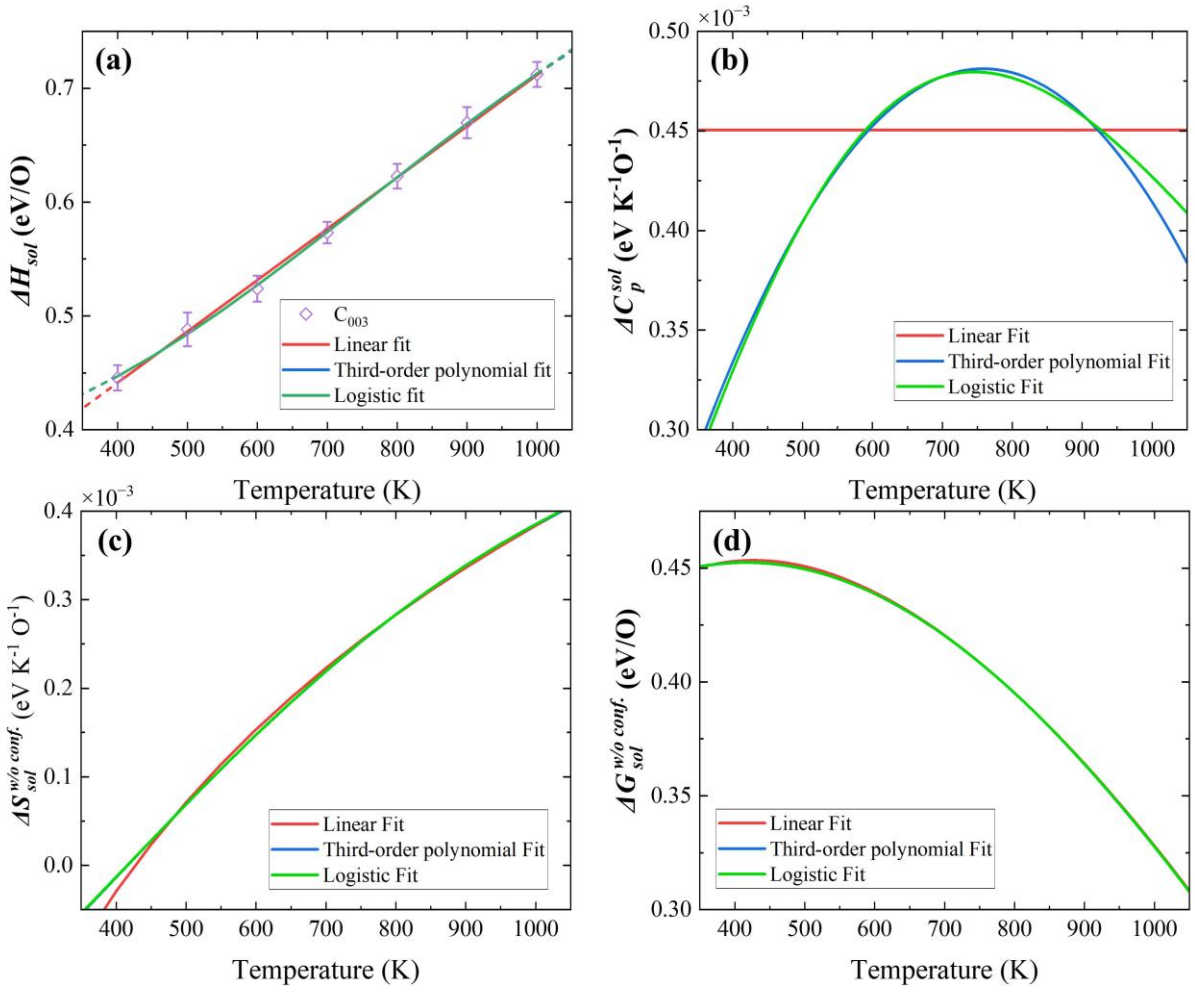

Figure S7. Thermodynamic quantities as functions of temperature, using linear, third-order polynomial and logistic fittings for solution enthalpy: (a) solid Na_2O solution enthalpy in liquid Na, (b) heat capacity of solution of solid Na_2O in

liquid Na, (c) solid Na_2O solution entropy in liquid Na excluding configurational entropy and (d) Gibbs free energy of solution excluding configurational entropy of solid Na_2O in liquid Na. In the case of the logistic function, numerical integration was applied to determine the solution entropy, as the analytical solution does not exist,

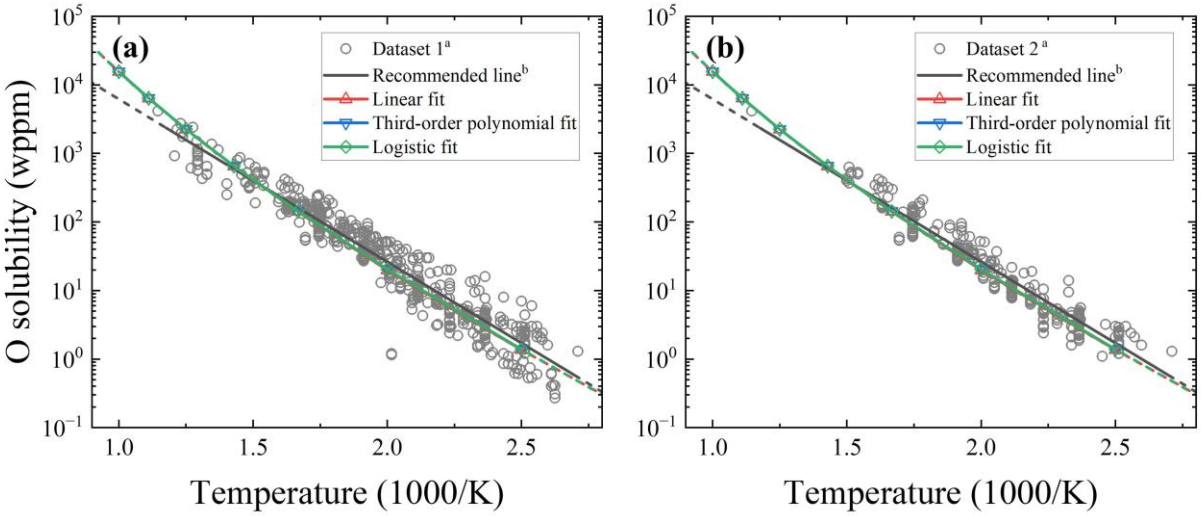

a. Reference[6]
b. Reference[7]

Figure S8. Theoretically predicted solubility curves using three fitting equations for solution enthalpy; (a) comparison with all available experimental data, which are called Dataset 1 in the main text and (b) comparison only with experimental data measured by vacuum distillation, which are called Dataset 2 in the main text. The dashed lines indicate extrapolation, while the solid lines show interpolation (400–1000 K).

S10. Effect of energy cutoff on the DFT calculation of the elastic constants of solid Na_2O

In Section 3.2 of the main text, the elastic constants of solid Na_2O calculated with the constructed MTPs are compared with previously published DFT data. Since our MTPs were fitted to calculation results of DFT–PBE, C_{11} and C_{44} were obtained consistent with previously reported DFT–GGA data.[8,9,10] However, for C_{12}, the reported DFT–GGA data themselves exhibited a large variance with a maximum difference of 22.1 GPa. One possible reason for the discrepancy is the plane wave energy cutoff, as three publications[8,9,10] used different values: 408 eV,[8] 520 eV[9] and 600 eV.[10] Therefore, to confirm the accuracy of calculated C_{12} with respect to the energy cutoff, we calculated the elastic constants with an energy cutoff of 400, 600 or 800 eV. For comparison, all calculations used the same k-point mesh (Γ-centered 5×5×5) and the same smearing width of the gaussian smearing method (0.05 eV), and the calculations were performed on the conventional cubic unit cell of solid Na_2O composed of 12 atoms. Figure S9 shows the calculated stress–strain relations and elastic constants when applying the strain in xx and xy directions. It is evident that 400 eV was insufficient and 600 eV was sufficient as the energy cutoff to precisely calculate the elastic constants. Therefore, we consider that the DFT calculation results reported in the study of Thompson et al.[8], which employed 408 eV energy cutoff, are inaccurate. Except for the data of Thompson et al., all previously reported DFT–GGA data are in reasonable agreement and our MTP gave elastic constants consistent with these DFT–GGA data, as described in the main text.

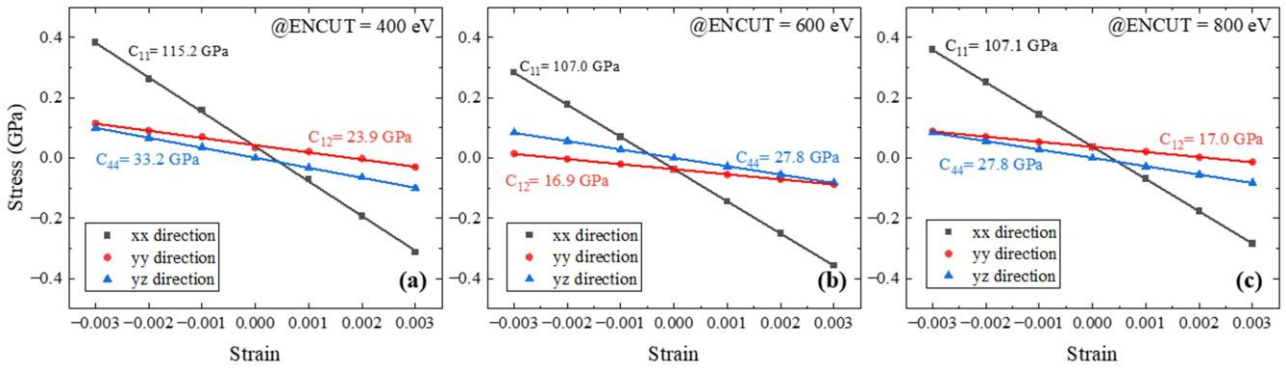

Figure S9. Stress–strain relations and elastic constants calculated with a planewave energy cutoff of (a) 400e V, (b) 600 eV or (c) 800 eV for solid Na_2O. Strain was applied in xx and xy directions.

S11. Test results of other correction methods for DFT systemic error

In addition to the correction presented in the main text, we tested several corrections to suppress the DFT systematic error, including (1) Grimme's D2 dispersion correction, (2) short-range Na–O attractive energy correction and (3) truncated Coulomb correction of Na–Na, Na–O and O–O combinations. Since DFT accurately predicts the bulk properties of liquid Na and solid Na_2O, the DFT systematic error correction should affect the O solubility in liquid Na but not the bulk properties. To evaluate the performance of corrections with respect to O solubility, we checked Na_2O solution enthalpy in liquid Na, as the direct coexistence method for O solubility requires substantial computational effort.

(1) Grimme's D2 dispersion correction

Grimme's D2 dispersion correction[11] was selected as an example of general dispersion correction methods. Since the D2 correction is pairwise, it can be easily combined with the untrained MTP ad hoc. Modern dispersion correction methods, such as Grimme's D4 dispersion correction,[12] may outperform the D2 correction. However, we left their tests for future work because modern corrections require entirely new DFT calculations for building the MTP training set.

Table S5 presents the Na_2O solution enthalpy in liquid Na calculated using MTP with the D2 correction at 600 and 1000 K, and compares them with the results of the uncorrected MTP, C_{003} and DFT–PBE. In the main text, it is confirmed that the solution enthalpy of approximately 0.5 eV/atom at 600 K resulted in consistent O solubility with the experiments. Compared with this value, the D2 correction causes an excess correction, resulting in an underestimation of O solubility. Therefore, the D2 correction is not suitable for the O solubility correction.

Table S5. Na_2O solution enthalpy in liquid Na at 600 and 1000 K, calculated by using C_{wo}, C_{003}, MTP with Grimme's D2 dispersion correction and DFT.

Solution enthalpy	600 K (eV/O)	1000 K (eV/O)
C_{wo}	0.357 ± 0.010	0.492 ± 0.012
C_{003}	0.524 ± 0.011	0.712 ± 0.011
MTP with Grimme's D2 correction	0.780 ± 0.009	0.858 ± 0.011
DFT–PBE [a]	0.296 ± 0.059	0.396 ± 0.077

a. Reference[13]

The density of liquid Na was also calculated as a representative bulk property of liquid Na using MTP with the D2 correction and is compared with that of the uncorrected MTP, DFT–PBE and experiments in Figure S10. The MTP with the D2 correction exhibited evident density overestimation, while all others were in good agreement with the experiments.

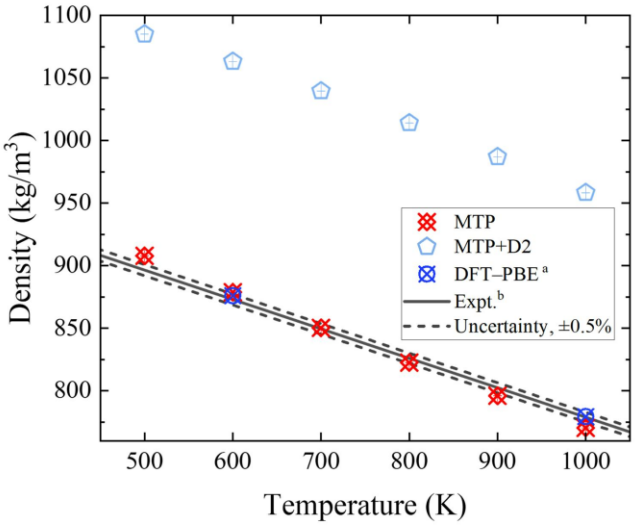

a. **Reference**[14]

b. **Reference**[15]

Figure S10. Density as a function of temperature for liquid Na calculated by using C_{wo}, MTP with Grimme's D2 dispersion correction, DFT–PBE, and experiments. The black dashed line indicates the 0.5 % uncertainty of experimental densities.

Finally, the pressure–volume relation of solid Na_2O at 300 K was calculated using the MTP with the D2 correction as a representative bulk property of solid Na_2O and is compared with that of the uncorrected MTP, C_{003} and experiments. Figure S11 shows that the D2 correction results in underestimation. Furthermore, the lattice constant and bulk modulus were calculated by fitting the pressure–volume relation to BM–EOS (Table S6), indicating significant errors.

In summary, Grimme's D2 dispersion correction is inappropriate for systems composed of liquid Na and solid Na_2O. Nonetheless, it is still worth considering the application of modern dispersion corrections in the future, particularly with the aim of simulating gas phase reactions, which are crucial in liquid Na combustion.

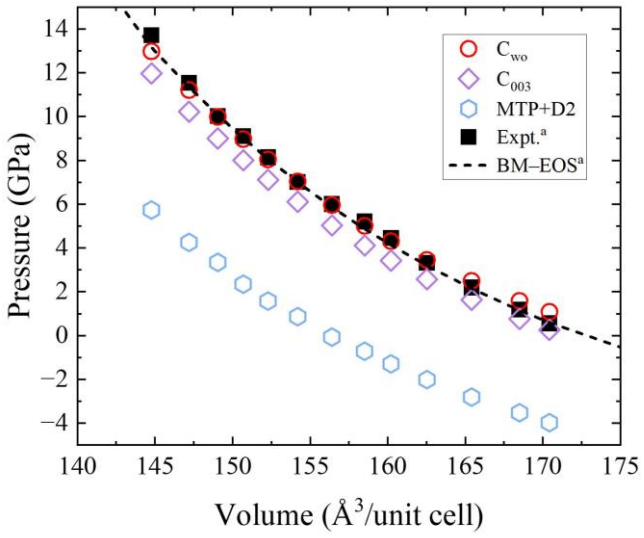

a. **Reference**[16]

Figure S11. Pressure–volume relation of solid Na_2O at 300 K as obtained by using C_{wo} C_{003}, MTP with Grimme's D2 dispersion correction and experiments. The dotted line indicates the BM–EOS derived from experimental data.

Table S6. Lattice constant and bulk modulus of solid Na_2O at 300 K obtained from BM–EOS fitting to the pressure–volume relation established by C_{wo}, C_{003}, MTP with Grimme's D2 dispersion correction and experiment.

	a (Å)	B_0 (GPa)
C_{wo}	5.60	35.26
C_{003}	5.56	39.84
MTP with Grimme's D2 correction	5.39	59.05
Expt.	5.568[a], 5.55[b]	44.1[a]

a. Reference[16]
b. Reference[17]

(2) Short-range Na–O attractive energy

Adding short-range Na–O attractive energy can be a possible correction to increase the solution enthalpy by stabilising solid Na_2O. The tested 2B correction for short-range Na–O attractive energy is expressed as follows,

$$f_{2B}(r) = \begin{cases} 0.0002(r-4.0)^3 r^{2.8} & r \le 4.0 \\ 0 & r > 4.0 \end{cases}, \quad \text{(S27)}$$

where r is the interatomic distance between Na and O atoms.

The functional form of this correction is depicted in Figure S12. The correction was designed to affect the energy near the first-neighbour distance between Na and O atoms in solid Na_2O, approximately 2.4 Å.

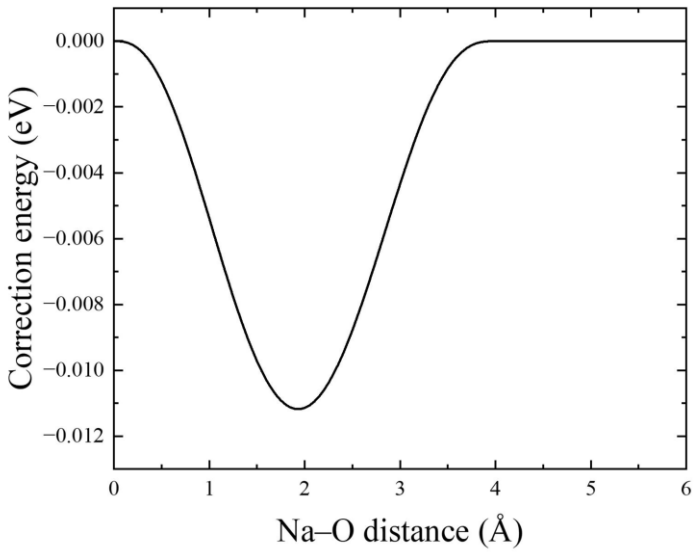

Figure S12. Potential energy curve of the short-range Na–O attractive correction as a function of the distance between Na and O atoms.

Table S7 shows a comparison of the Na_2O solution enthalpy in liquid Na using the uncorrected MTP, C_{003}, MTP with the short-range Na–O energy correction and DFT–PBE. The Na–O energy correction fails to increase the solution enthalpy and induces just a minor change. It is because the O impurity in liquid Na is additionally stabilised in a comparable degree with O in solid Na_2O as the short-range Na–O interaction per O atom can similarly occur in both cases. In addition, the Na–O energy correction undermined the reproductivity of the bulk properties of solid Na_2O, which are well reproduced by the uncorrected MTP. Therefore, the short-range Na–O energy correction is unsuitable for the present study, although there may be a better formula that can increase Na_2O solution enthalpy.

Table S7. Na_2O solution enthalpy in liquid Na calculated by C_{wo}, C_{003}, MTP with short-range Na–O energy correction and DFT at 600 and 1000 K.

	600 K (eV/O)	1000 K (eV/O)
C_{wo}	0.357 ± 0.010	0.492 ± 0.012
C_{003}	0.524 ± 0.011	0.712 ± 0.011
MTP with short-range Na–O energy correction	0.354 ± 0.012	0.540 ± 0.016
DFT–PBE [a]	0.296 ± 0.059	0.396 ± 0.077

a. Reference[13]

(3) Truncated Coulomb interaction of all Na–Na, Na–O and O–O combinations

Since some of our systems involve Coulomb interactions between ions, we also tested a correction in the form of truncated Coulomb interaction for all pairwise combinations. Specifically, the modified version of Wolf summation method[18] proposed by Fennell et al.[19] was used:

$$\mathrm{E} = 14.4 q_i q_j \left[\frac{erfc(\alpha r)}{r} - \frac{erfc(\alpha r_c)}{r_c} + \left(\frac{erfc(\alpha r_c)}{r_c^2} + \frac{2\alpha}{\sqrt{\pi}} \frac{\exp(-\alpha^2 r_c^2)}{r_c} \right) (r - r_c) \right] \quad r < r_c, \tag{S28}$$

where erfc is the complementary error function, α is the damping parameter, r_c is the cutoff radius, q_i and q_j are the charges of atom type i and j, respectively, and r is the interatomic distance between type i and type j atoms. Here we present the results of the correction using α = 0.1, r_c = 6 Å, q_{Na} = 0.15 and $q_O = -0.3$. Figure S13 shows the functional shape of this correction of all Na–Na, Na–O and O–O combinations.

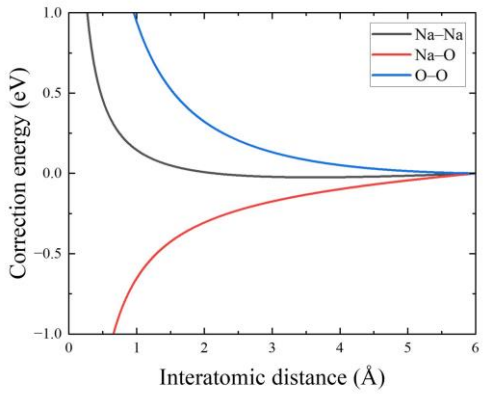

Figure S13. Potential energy curve of the truncated Coulomb correction applied to all combinations of Na–Na, Na–O and O–O, with the interatomic distance between each combination.

The comparison of the Na_2O solution enthalpy in liquid Na calculated using the C_{wo}, C_{003}, MTP with the truncated Coulomb correction and DFT–PBE is presented in Table S8. The truncated Coulomb correction results in further underestimation of the solution enthalpy, as Na–O interaction occurs more frequently in "an O impurity in liquid Na" than in "O in solid Na_2O". In addition, this correction undermined the reproductivity of the bulk properties of solid Na_2O and liquid Na, which are well reproduced by the uncorrected MTP. Therefore, the correction is deemed unsuitable.

Table S8. Comparison of Na_2O solution enthalpy in liquid Na calculated by C_{wo}, C_{003}, MTP with truncated Coulomb correction and DFT–PBE at 600 and 1000 K.

	600 K (eV/O)	1000 K (eV/O)

C_{wo}	0.357 ± 0.010	0.492 ± 0.012
C_{003}	0.524 ± 0.011	0.712 ± 0.011
MTP with truncated Coulomb correction	0.238 ± 0.010	0.434 ± 0.012
DFT–PBE [10]	0.296 ± 0.059	0.396 ± 0.077

a. Reference[13]

Based on the test results of various correction methods, including the three methods presented in this section, we finally concluded that the O–O attractive energy correction is the most simple and effective correction for systems composed of liquid Na and solid Na_2O to simultaneously reproduce various bulk properties and O solubility and diffusivity, as presented in the main text. Nevertheless, since the O–O attractive energy correction is not a general correction, finding a general correction remains a significant challenge for future work to realise accurate simulations of liquid Na combustion, as discussed in Section 3.7 of the main text.

S12. Potential model files and implementation of the 2B correction in LAMMPS package

In LAMMPS package,[5] multiple potential models can be combined by using the "hybrid" bond style. To apply the 2B correction, we constructed a file that lists energy and force values as a function of interatomic distances in the readable "table" bond style. For the use of C_{003}, we combine the two potential models: the uncorrected MTP and the 2B correction potential. The following is an example of how to use C_{003} in LAMMPS.

```
pair_style hybrid/overlay table linear 1000  mlip mlip.ini
pair_coeff 2 2  table 2b_003.table TABLE_2B 6.0

pair_coeff * *   mlip mlip.ini
```

Elements 1 and 2 represent Na and O, respectively. The following is an example of mlip.ini file.

```
mtp-filename    pot16_Na-O.mtp
```

The uncorrected MTP file (pot16_Na-O.mtp) and the 2B correction table file (2b_003.table) are shared as a part of the supporting information to facilitate the reproduction of the present results and future use of the constructed potential model. The files are available at https://github.com/Chae-yeongKim/MTP_for_binary_Na-O_system.

S13. MTP validation for reproductivity of DFT–PBE results

In the training of MTPs, we utilized the "structures" weighting method of MLIP package[3], by which the loss function is defined as

$$\sum_{k=1}^{K}\Big[\frac{w_e}{(N_k)^2}\left(E^{mtp}(cfg_k;\theta)-E^{qm}(cfg_k)\right)^2+\frac{w_f}{N_k}\sum_{i=1}^{N_k}\left|f_i^{mtp}(cfg_k;\theta)-f_i^{qm}(cfg_k)\right|^2 + \frac{w_s}{(N_k)^2}\left(\sigma^{mtp}(cfg_k;\theta)-\sigma^{qm}(cfg_k)\right)^2\Big]\rightarrow min, \quad \text{(S29)}$$

where K is the number of configurations in training set, N_k is the number of atoms in the k[th] configuration and w_e, w_f and w_s are weights expressing the relative importance of energy, force and stress data. These weights were set to be 1, 0.01 and 0.001, which are the default values of MLIP package. $E^{mtp}(cfg_k;\theta)$, $f_i^{mtp}(cfg_k;\theta)$ and $\sigma^{mtp}(cfg_k;\theta)$ are energy, force of the i[th] atom and stress in the k[th] configuration, obtained by MTP with a set of fitting coefficients θ. $E^{qm}(cfg_k)$, $f_i^{qm}(cfg_k)$ and $\sigma^{qm}(cfg_k)$ are energy, force of the i[th] atom and stress data calculated by DFT–PBE for the same configuration.

Table S9 shows RMSEs of per-atom energy in the training data used in the supervised learning. The MTP reproduced the DFT reference data well with an average training error of 1.84 meV/atom. Although the 12-atom perfect solid Na_2O and Na/O atom calculations have relatively large energy errors due to the relatively small number of configurations contained in them, we consider these errors acceptable for the following reasons. First, as confirmed in Table 1 of the main text, the MTP reasonably reproduces the DFT results for the lattice and elastic constants of solid Na_2O. The

12-atom solid Na_2O data were added to better describe these properties, which was successfully achieved. Next, the error for each atomic energy is shown in Table S10. The main properties affected by these errors are Na cohesive energy and O_2 binding energy. The propagation errors are only 0.015 eV and 0.018 eV for Na cohesive and O_2 binding energy, respectively. In addition, the atomic state does not occur in the systems of interest in the present study. Thus, we also consider this error to be acceptable. In conclusion, the MTP (without the 2B correction) reproduced well the DFT results used as the training set.

Table S9. RMSEs of energy and force of the systems used in the supervised learning.

Reference Data		Number of configurations	Number of atoms	RMSE of energy (meV/atom)	RMSE of force (eV/Å)
Perfect solid Na_2O	✓ Static calculation ✓ Strain was applied in xx and xy directions.	203	12	6.82	0.007
	✓ *NVT*, FPMD ✓ 300 K, 1200 K	800	96	0.57	0.020
Solid Na_2O containing 3 vacancies ($2V_{Na}1V_O$)	✓ *NVT*, FPMD ✓ 300 K, 800 K, 1200 K	440	93	2.52	0.040
Liquid pure Na	✓ *NVT*, FPMD ✓ 600 K, 1000 K, 2000 K, 4000 K	1250	102	0.91	0.015
Liquid Na surface	✓ *NVT*, FPMD ✓ 600 K, 1000 K, 1500 K, 2000 K	1000	102	1.31	0.019
Liquid Na with O impurity	✓ *NVT*, FPMD ✓ O impurity concentrations: $Na_{101}O_1$, $Na_{100}O_2$, $Na_{98}O_4$, $Na_{96}O_6$, $Na_{94}O_8$, $Na_{92}O_{10}$ ✓ 600 K, 1000 K, 2000 K, 4000 K	2150	102	1.84	0.028
Liquid Na_2O	✓ *NVT*, FPMD ✓ 600 K, 1000 K, 2000 K, 4000 K	1200	96	1.03	0.047
Interfaces between liquid Na and solid Na_2O	✓ *NVT*, FPMD ✓ 600 K, 1000 K, 1500 K, 2000 K ✓ Crystal orientation of Na_2O: (100), (110), (111)	1520	189 for (100) interface, 146 for (110) interface, 118 for (111) interface	1.69	0.042
Na/O atom	✓ Static calculation	2	1	12.23	0.001
Total		8565	-	1.82	0.033

Table S10. Energy of Na and O atoms calculated using DFT–PBE and MTP.

	DFT–PBE (eV/atom)	MTP (eV/atom)	Difference (eV/atom)
Na atom	-0.226	-0.241	-0.015
O atom	-1.532	-1.540	-0.009

Test error was also checked to evaluate whether the MTP model can reproduce DFT–PBE for configurations that were not included in the training data. The following four systems were tested: (1) liquid Na at 800 K, (2) solid Na_2O at 300 K, (3) solid Na_2O at 800 K and (4) interface between liquid Na and solid Na_2O at 800 K. The interface is a (100) interface system whose initial composition is $Na_{45(l)}$-$Na_{96}O_{48(s)}$. In each test system, MD simulation using the MTP (without the 2B correction) was first performed by LAMMPS code for 100 ps and atomistic configurations were extracted every 1 ps. Subsequently, DFT–PBE static calculations were performed on these 100 configurations for each system. The default setting listed in Table S2 was utilized in the DFT calculations and the numerical error correction was applied to compare with MTP. Figure S14

exhibits the energy comparison between MTP and DFT–PBE and demonstrates that MTP can reasonably reproduce DFT–PBE for four different test cases. The relatively large error in the interface simulation comes from the fact that Na_2O dissolution occurred significantly, as the 2B correction was not applied in this test to evaluate the performance of the as-trained MTP. Nevertheless, the error in this chemically complex system is still reasonably small: an RMSE of 3.51 meV/atom for per-atom energy.

Lastly, Figure S15 shows RMSEs of atomic forces in the test calculations. Good agreement between DFT and MTP was confirmed. The fact that the force error in the training data is close to that in the test data indicates that overfitting did not occur.

Considering the training and test errors evaluated, we conclude that the MTP achieved DFT accuracy in energy and force calculations.

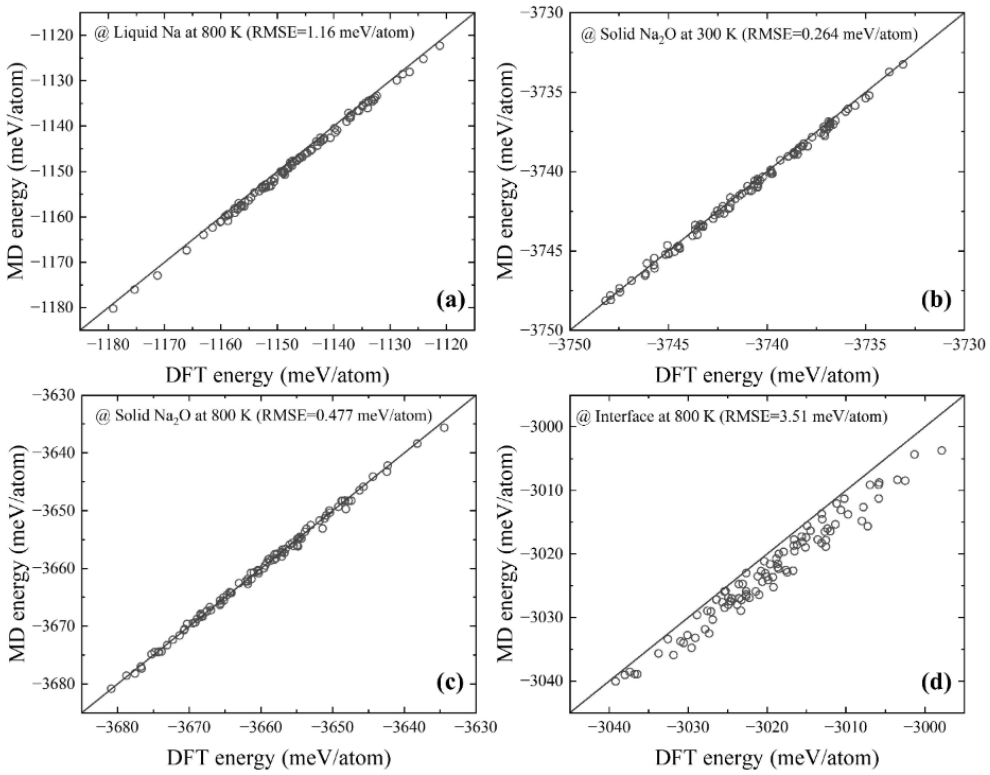

Figure S14. Potential energies calculated using MTP and DFT–PBE for atomic configurations selected from MTP-driven MD simulations: (a) liquid Na at 800 K, (b) solid Na_2O at 300 K, (c) solid Na_2O at 800 K and (c) interface at 800 K. The RMSE of per-atom energy is shown at the top of each figure.

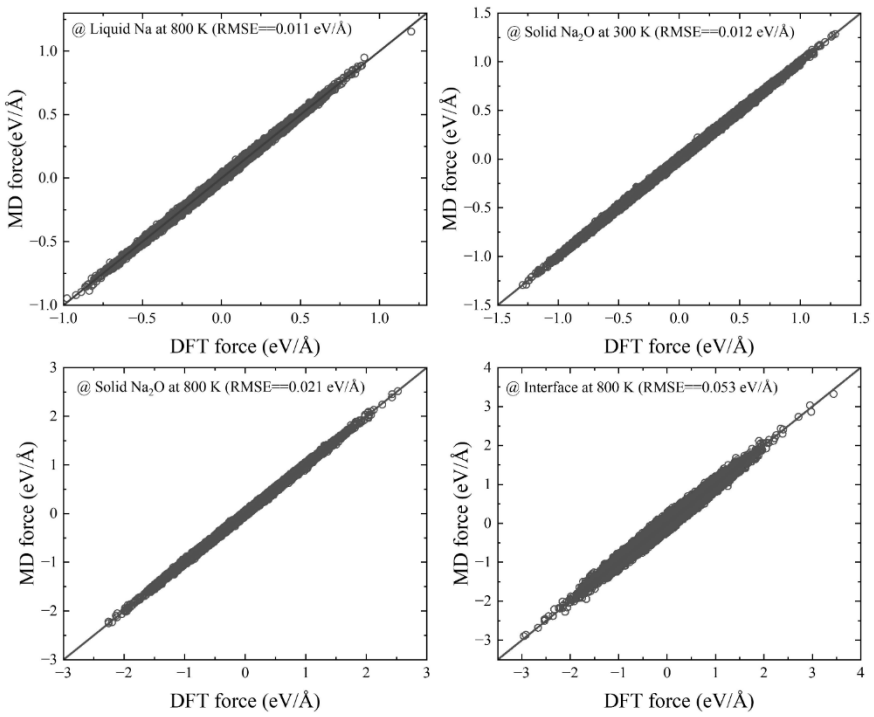

Figure S15. Atomic forces calculated using MTP and DFT–PBE for atomic configurations selected from MTP-driven MD simulations: (a) liquid Na at 300 K, (b) solid Na_2O at 300 K, (c) solid Na_2O at 800 K and (c) interface. The RMSE of force is shown at the top of each figure.

S14. Preliminary assessment of the performance of r^{2}SCAN on O solubility calculation

The 2B correction improves the prediction of O solubility in liquid Na by increasing the stability of $Na_2O_{(s)}$, indicating that O solubility can be better calculated using an exchange-correlation functional that stabilizes $Na_2O_{(s)}$ compared to the PBE function. Here, we tested r^{2}SCAN,[20] one of the most widely used meta-GGA functionals, which generally outperforms PBE in the calculation of metal oxide formation enthalpies[21].

According to our previous study,[22] the energy of solid Na_2O in reference to an isolated O atom and liquid Na is relevant to the accuracy of Na_2O solution enthalpy calculation in liquid Na. Since the enthalpy difference between liquid Na and solid Na is almost independent of the exchange-correlation functional,[23] liquid Na enthalpy can be replaced with solid Na enthalpy to simplify the calculation.

In Table S11, r^{2}SCAN is compared with PBE for the energy of $Na_2O_{(s)}$ in reference to solid Na and O atom (ΔE_{Na_2O}) as well as for $O_{2\,(g)}$ binding energy, $Na_2O_{(s)}$ formation energy and $Na_{(s)}$ atomization energy. r^{2}SCAN generally outperforms PBE. The difference in ΔE_{Na_2O} between r^{2}SCAN and PBE indicates that r^{2}SCAN stabilizes $Na_2O_{(s)}$ by 0.27 eV/O atom compared to PBE. 0.27 eV/O atom is comparable with the change due to the C_{003} correction at 600 K (0.17 eV/O atom). Hence, with r^{2}SCAN, no correction is needed or a smaller correction may be sufficient. We plan to construct an MTP with r^{2}SCAN and evaluate its performance in the future.

Table S11. Comparison between PBE and r^{2}SCAN for energies related to the stability of $Na_2O_{(s)}$ solution in liquid Na.

	PBE	r^{2}SCAN	Experiment
Formation energy of $Na_2O_{(s)}$ (eV)	3.783	4.375	4.332[a]
Binding energy of $O_{2(g)}$ (eV)	6.079	5.431	5.231[b]
Atomization energy of $Na_{(s)}$ (eV)	1.072	1.075	1.113[c]
Energy of $Na_2O_{(s)}$ in reference to $Na_{(s)}$ and O atom (eV)	6.822	7.091	6.945[d]

a. The standard enthalpy of formation at 298.15 K[24].
b. The zero-point vibration effect is excluded so that it can be directly compared to the DFT calculation results[13].
c. Energy required to separate the solid to neutral atoms in ground electronic state at 0 K and 1 atm.[25]

d. This value was obtained as $4.332 + \frac{5.231}{2}$.[24]

References

(1) Kresse, G.; Furthmüller, J. Efficient Iterative Schemes for Ab Initio Total-Energy Calculations Using a Plane-Wave Basis Set. *Phys. Rev. B* **1996**, *54* (16), 11169–11186. https://doi.org/10.1103/PhysRevB.54.11169.

(2) Pack, H. J. M. and J. D. Special Points for Brillonin-Zone Integrations. **1976**, *7* (5), 5188–5192. https://doi.org/https://doi.org/10.1103/PhysRevB.13.5188.

(3) Novikov, I. S.; Gubaev, K.; Podryabinkin, E. V; Shapeev, A. V. The MLIP Package: Moment Tensor Potentials with MPI and Active Learning. *Mach. Learn. Sci. Technol.* **2021**, *2* (2), 025002. https://doi.org/10.1088/2632-2153/abc9fe.

(4) Shapeev, A. V. Moment Tensor Potentials: A Class of Systematically Improvable Interatomic Potentials. *Multiscale Model. \& Simul.* **2016**, *14* (3), 1153–1173. https://doi.org/10.1137/15M1054183.

(5) Thompson, A. P.; Aktulga, H. M.; Berger, R.; Bolintineanu, D. S.; Brown, W. M.; Crozier, P. S.; in 't Veld, P. J.; Kohlmeyer, A.; Moore, S. G.; Nguyen, T. D.; Shan, R.; Stevens, M. J.; Tranchida, J.; Trott, C.; Plimpton, S. J. LAMMPS - a Flexible Simulation Tool for Particle-Based Materials Modeling at the Atomic, Meso, and Continuum Scales. *Comput. Phys. Commun.* **2022**, *271*, 108171. https://doi.org/10.1016/j.cpc.2021.108171.

(6) Borgstedt, H. U.; Guminski, C.; Borgstedt, H. U.; Guminski, C. IUPAC-NIST Solubility Data Series. 75. Nonmetals in Liquid Alkali Metals. *J. Phys. Chem. Ref. Data* **2001**, *30* (4), 835–1158. https://doi.org/10.1063/1.1391426.

(7) Eichelberger, R. L. *THE SOLUBILITY OF OXYGEN IN LIQUID SODIUM: A RECOMMENDED EXPRESSION*; AI-AEC-12685; US Atomic Energy Commision, Atomics International: Canoga Park, CA, 1968. https://www.osti.gov/biblio/4808140 (accessed 2022-11-12).

(8) Thompson, M.; Shen, X.; Allen, P. B. Density Functional Calculation of Electronic Structure and Phonon Spectra of Na2O. *Phys. Rev. B* **2009**, *79* (11), 113108. https://doi.org/10.1103/PhysRevB.79.113108.

(9) Noinonmueng, T.; Phacheerak, K. Structural and Mechanical Properties of Cubic Na2O: First-Principles Calculations. *JARST* **2020**, *19* (2), 17–24.

(10) Phacheerak, K.; Thanomngam, P. Pressure Dependence of Structural and Elastic Properties of Na 2 O: First-Principles Calculations. *Integr. Ferroelectr.* **2022**, *224* (1), 256–263. https://doi.org/10.1080/10584587.2022.2035615.

(11) Grimme, S. Semiempirical GGA-Type Density Functional Constructed with a Long-Range Dispersion Correction. *J. Comput. Chem.* **2006**, *27* (15), 1787–1799. https://doi.org/10.1002/jcc.20495.

(12) Caldeweyher, E.; Ehlert, S.; Hansen, A.; Neugebauer, H.; Spicher, S.; Bannwarth, C.; Grimme, S. A Generally Applicable Atomic-Charge Dependent London Dispersion Correction. *J. Chem. Phys.* **2019**, *150* (15). https://doi.org/10.1063/1.5090222.

(13) Gil, J.; Oda, T. Solution Enthalpy Calculation for Impurity in Liquid Metal by First-Principles Calculations: A Benchmark Test for Oxygen Impurity in Liquid Sodium. *J. Chem. Phys.* **2020**, *152* (15), 154503. https://doi.org/10.1063/1.5136324.

(14) Han, J.-H.; Oda, T. Performance of Exchange-Correlation Functionals in Density Functional Theory Calculations for Liquid Metal: A Benchmark Test for Sodium. *J. Chem. Phys.* **2018**, *148* (14), 144501. https://doi.org/10.1063/1.5017198.

(15) Sobolev, V. *Database of Thermophysical Properties of Liquid Metal Coolants for GEN-IV*; SCK•CEN-BLG-1069; Belgian Nuclear Research Centre (SCK•CEN): Belgium, 2011. https://inis.iaea.org/search/search.aspx?orig_q=RN:43095088 (accessed 2022-11-12).

(16) Wu, X.; Zhang, Y.; Zhang, J.; Liu, R.; Yang, J.; Yang, B.; Xu, H.; Ma, Y. High Pressure X-Ray Diffraction Study of Sodium Oxide (Na2O): Observations of Amorphization and Equation of State Measurements to 15.9 GPa. *J. Alloys Compd.* **2020**, *823*, 153793. https://doi.org/10.1016/j.jallcom.2020.153793.

(17) Zintl, E.; Harder, A.; Dauth, B. Gitterstruktur Der Oxyde, Sulfide, Selenide Und Telluride Des Lithiums, Natriums Und Kaliums. *Zeitschrift für Elektrochemie und Angew. Phys. Chemie* **1934**, *40* (8), 588–593. https://doi.org/10.1002/bbpc.19340400811.

(18) Wolf, D.; Keblinski, P.; Phillpot, S. R.; Eggebrecht, J. Exact Method for the Simulation of Coulombic Systems by Spherically Truncated, Pairwise r-1 Summation. *J. Chem. Phys.* **1999**, *110* (17), 8254–8282. https://doi.org/10.1063/1.478738.

(19) Fennell, C. J.; Gezelter, J. D. Is the Ewald Summation Still Necessary? Pairwise Alternatives to the Accepted Standard for Long-Range Electrostatics. *J. Chem. Phys.* **2006**, *124* (23). https://doi.org/10.1063/1.2206581.

(20) Furness, J. W.; Kaplan, A. D.; Ning, J.; Perdew, J. P.; Sun, J. Accurate and Numerically Efficient R2SCAN Meta-Generalized Gradient Approximation. *J. Phys. Chem. Lett.* **2020**, *11* (19), 8208–8215. https://doi.org/10.1021/acs.jpclett.0c02405.

(21) Kothakonda, M.; Kaplan, A. D.; Isaacs, E. B.; Bartel, C. J.; Furness, J. W.; Ning, J.; Wolverton, C.; Perdew, J. P.; Sun, J. Testing the R2SCAN Density Functional for the Thermodynamic Stability of Solids with and without a van Der Waals Correction. *ACS Mater. Au* **2022**. https://doi.org/10.1021/acsmaterialsau.2c00059.

(22) Gil, J.; Oda, T. Correction Methods for First-Principles Calculations of the Solution Enthalpy of Gases and Compounds in Liquid Metals. *Phys. Chem. Chem. Phys.* **2022**, *24* (2), 757–770. https://doi.org/10.1039/d1cp02450g.

(23) Han, J.-H.; Oda, T. Performance of Exchange-Correlation Functionals in Density Functional Theory Calculations for Liquid Metal: A Benchmark Test for Sodium. *J. Chem. Phys.* **2018**, *148* (14), 144501.

(24) Chase, M. NIST-JANAF Thermochemical Tables, 4th Edition. American Institute of Physics, -1 1998.

(25) Brewer, L. *THE COHESIVE ENERGIES OF THE ELEMENTS*; LBNL Report: LBL-3720; Lawrence Berkeley National Laboratory: CA, 1977. Rev. Retrieved from https://escholarship.org/uc/item/08p2578m (accessed 2023-06-23).